CONFERENCE PRE-PRINT

EFFECT OF ECH ON ENERGETIC-PARTICLE-DRIVEN MHD MODES IN HELIOTRON J

K. NAGASAKI, S. KOBAYASHI, S. INAGAKI, S. KADO, S. I. INAGAKI, S. KONOSHIMA, T. MIZUUCHI
Institute of Advanced Energy, Kyoto University
Gokasho, Uji, Kyoto, Japan
Email: nagasaki.kazunobu.4x@kyoto-u.ac.jp

Y. ZHONG, Z. WANG, J. CHEN
Sino-French Institute of Nuclear Engineering and Technology, Sun Yat-sen University
Zhuhai 519082, China

J. VARELA
University of Texas, U.S.A.

Y. NAKAMURA***, A. MATSUYAMA***, A. ISHIZAWA***
Graduate School of Energy Science, Kyoto University, Kyoto, Japan

P. ADULSIRISWAD
National Institutes for Quantum Science and Technology, Aomori, Japan

Abstract

Energetic-particle (EP)-driven MHD modes are studied experimentally and theoretically in the Heliotron J stellarator/heliotron device. Experiments scanning magnetic field configurations and electron cyclotron heating (ECH) power have demonstrated that the excitation and suppression of the global Alfvén eigenmode (GAE) and the energetic particle mode (EPM) depend on the bumpiness (toroidal mirror ripple) of the magnetic field configuration. The ECH effect varies depending on the mode being excited. For specific modes, an optimal ECH power exists for suppression, as the mode intensity decreases most significantly at a certain ECH power. The experimental results are compared with a linear simulation using the FAR3d code. The radial profile of a main mode measured with a beam emission spectroscopy (BES) showed a multi-peak radial structure, consistent with eigenvalue calculations using the FAR3d code. The mode intensity is determined by balance between the growth rate by energetic ion pressure, β_f and the damping rate by thermal electron pressure, β_{th}. The effect of trapped electrons generated by ECH is also discussed.

1. INTRODUCTION

In magnetically confined fusion plasmas, energetic particles (EPs) generated by D–T fusion reactions and plasma heating excite EP-driven magnetohydrodynamic (MHD) modes through the gradient of the EP distribution function in the resonance region. In tokamaks and stellarator/heliotron (S/H) devices, instabilities such as Alfvén eigenmodes (AEs) and energetic particle modes (EPMs) have been experimentally observed [1][2][3][4]. These modes enhance anomalous transport of EP and induce EP losses, thereby reducing heating efficiency and causing detrimental effects such as first wall damage. Conversely, the MHD waves are applicable to MHD spectroscopy [5][6] and hold potential for measuring safety factor and deuterium-tritium ratios, as well as enabling direct ion heating by energetic particles via α-channelling [7][8]. Therefore, controlling EP-excited MHD instabilities and understanding their physical mechanisms represent critical challenges in fusion energy research.

Several external actuators for controlling and stabilizing EP drive modes have been proposed and demonstrated [9]. Promising control techniques include: (i) modifying the gradient of the energetic ion distribution by varying the ion source [10][11][12][13][14][15], (ii) modifying the energetic ion distribution using localized electron cyclotron heating (ECH) [16][17][18][19][20][21][22][23], (iii) modifying the equilibrium state through localized electron cyclotron current drive (ECCD) [24][25], and (iv) applying an external 3-D perturbation magnetic field to manipulate the energetic ion distribution and wave drive [26][27]. These techniques have been proposed and experimentally tested.

Electron cyclotron heating (ECH) and electron cyclotron current drive (ECCD) are ideal stabilization tools since they can provide highly localized electron cyclotron (EC) power and current with good controllability at known positions [28]. ECCD can locally vary the magnetic shear, thus control mode damping. Because S/H devices have

low toroidal current, ECCD can generate a significant portion of the total plasma current, making it easy to observe the effect of ECCD on AE activity. On the Heliotron J device, both co- and counter-ECCD were demonstrated to stabilize energetic particle modes (EPMs) and global AE (GAE) [24][25]. Multiple experiments in the TJ-II, Heliotron J and LHD devices confirmed the fundamental physical mechanisms for the mitigation and suppression of EP-driven modes [29][30][31].

ECH can locally alter plasma distributions and utilize diverse interactions. Since AE is extremely sensitive to q profile, electron density and temperature profiles, ECH strongly influences excitation and damping, and consequently stability. Experiments on DIII-D and AUG showed that ECRF heating mitigated [32] or suppressed reverse-shear AE (RSAE) in discharges with initial NBI heating and an elevated reversed q profile [33][34]. On the TJ-II device, applying ECH power to the neutral beam injection (NBI) plasma was confirmed to alter AE behaviour [21]. The ECH effect on GAEs and EPMs was theoretically studied using the FAR3d code in Heliotron J [35]. Furthermore, ECH power modulation experiments on Heliotron J observed a delay in the mode's responsiveness to ECH modulation [35]. The difference in bulk electron pressure during ECH rise and fall suggests that mode suppression is related not only to bulk plasma pressure but also to energetic ion confinement.

In this paper, we report control of EP-driven MHD modes with ECH in a S/H device, Heliotron J. We employ ECH to tangential NBI-heated plasmas, which excite EP-driven MHD modes, including GAEs and EPMs. We study the effect of ECH on the magnetic configuration, particularly the bumpiness (toroidal mirror ripple). The experimental results are compared with a linear simulation using FAR3d code to investigate the excitation and damping terms. The paper is organized as follows. The EP-driven modes in Heliotron J are described in Sec. 2. Experimental results on the ECH effect are shown in Sec. 3, and comparison with FAR3d code simulation is shown in Sec. 4. Conclusion is given in Sec. 5.

2. EP-DRIVEN MHD MODES IN HELIOTRON J

Heliotron J is a medium-sized S/H device [37][38]. The device has a major radius of R = 1.2 m, a minor radius of a ~ 0.2 m, and a magnetic field strength up to B = 1.5 T. The coil system consists of a continuous helical field coil (HFC) with the pole number of L = 1 and the toroidal pitch number of M = 4, two types of toroidal coils (TFC-A and TFC-B), and three sets of vertical coils. By adjusting the current in each coil, Heliotron J achieves the flexible magnetic field configuration. The magnetic field spectrum of Heliotron J is primarily composed of toroidicity, helicity, and bumpiness. Here the bumpiness is the toroidal mirror ripple component of the magnetic field, defined as $\varepsilon_b = B_{14}/B_{00}$, which is introduced to reduce neoclassical transport. The study in this paper investigates the effect of the magnetic field configuration for EP-driven modes. Three configurations are selected: high-bumpiness (HB, $\varepsilon_b = 0.15$), medium-bumpiness (MB, $\varepsilon_b = 0.06$), and low-bumpiness (LB, $\varepsilon_b = 0.01$) configurations [39], where ε_b is defined as the bumpiness at r/a = 0.6. The rotational transformation is $\iota/2\pi$ = 0.57 in vacuum for all configurations with weak shear ($s = a/\iota \, d\iota/dr < 0.02$). The plasma volume is nearly the same. The magnetic well is formed throughout the entire plasma region, providing good MHD stability against pressure-driven MHD instabilities. No interchange-type modes have been observed in the experiments of this study.

Plasmas are generated and heated by a second harmonic X-mode 70 GHz ECH system. The maximum ECH injection power is 350 kW. By setting the EC injection angle to $N_{\parallel}$ = 0.0, the EC current is barely driven. The magnetic field strength, B ~ 1.25 T, is configured to achieve an off-axis ECH power absorption profile (r/a ~ 0.3). The neutral beam injection (NBI) system employs two systems for co-injection and counter-injection using hydrogen, each with injection energy of E < 27 keV and the power of P_{NB} < 700 kW. Electron density is measured with a 130 GHz microwave interferometer, and electron density and temperature profiles are measured with a YAG Thomson scattering measurement system. The mode number is evaluated using magnetic probes, and the radial profile of modes is estimated from electron density fluctuation measurements with a beam emission spectroscopy (BES) diagnostic. Deuterium is used as the working gas.

EP-driven MHD modes are commonly observed in both tokamak and S/H devices. Modes excited by poloidal mode coupling such as TAE in S/H devices show no significant difference from modes in tokamak devices [3]. The difference between tokamaks and S/H devices relates to their magnetic field structure: tokamaks are ideally two-dimensional (2D) and axisymmetric, whereas S/H devices are three-dimensional (3D). In S/H devices, spectral gaps arising from both poloidal and toroidal mode couplings can excite EP-driven MHD modes such as HAE. The rotational transform profile influences the mode structure and growth rate. To identify the type of EP-driven MHD instability, the shear Alfvén spectrum structure of the Heliotron J device is calculated using the STELLGAP code [40]. Figure 1 shows the spectra for two cases: the plasma current of I_p = 0.0 kA and I_p = 0.5 kA. When no plasma current flows, the profiles of continua are almost flat, and no spectral crossings are observed.

Due to the low magnetic shear in the rotational transform profile, gap modes such as the toroidal Alfvén eigenmode (TAE) are not excited, but the global Alfvén eigenmode (GAE) and EP mode (EPM) are excited. When the plasma current flows, the magnetic shear in the rotational transform profile increases, the continua are reconfigured, and spectral line crossings and the expansion of the gap structure occur. However, the plasma current of 0.5 kA is weak in the experiments reported here, resulting in weak magnetic shear and a flat, continuous spectrum with few spectral crossings.

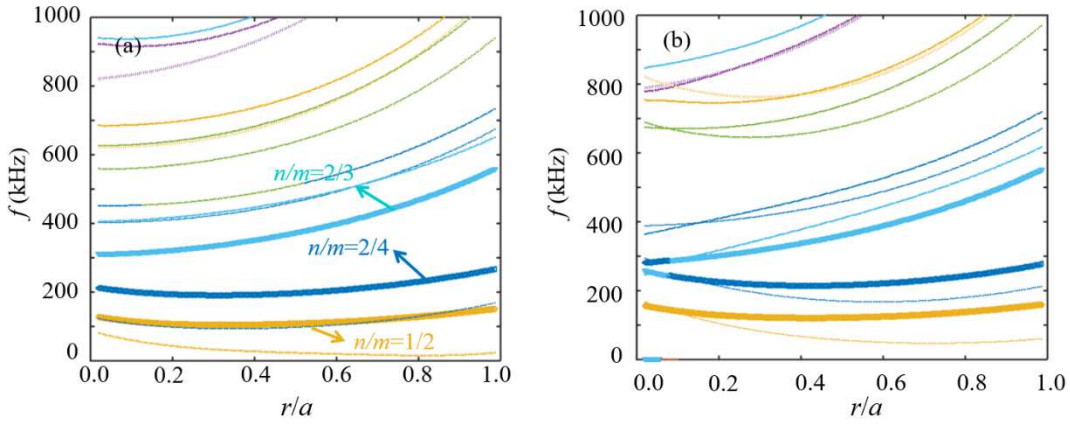

Fig. 1 Shear Alfvén spectra in Heliotron J, (a) Ip=0.0 kA and (b) Ip = 0.5 kA

3. EXPERIMENTAL RESULTS

We have conducted plasma experiments to investigate the response of EP-driven modes excited by NBI to ECH in Heliotron J. Figure 2 shows the magnetic power density spectrum for the MB configuration. Plasmas are produced by the ECH, and then the NB power is superposed. The electron density is gradually increased to $n_e = 0.6 \times 10^{19}$ m^{-3} during the discharge, and NB power is fixed at P_{BL1} = 400 kW, and P_{BL2} = 250 kW. The EC power is scanned in the range of 109 to 308 kW. To exclude ECCD effects on the observed modes, $N_{\parallel}$ is fixed at 0.0 so that the plasma current is kept low, I_p = 0.5 kA. The central electron temperature, $T_e(0)$ ranges from 0.4 to 0.9 keV, depending on the EC power. It can be seen that several modes are excited in the wide frequency range. The electron density gradually increases during discharge, and accordingly, modes above 150 kHz show a gradual decrease in frequency, suggesting GAE. On the other hand, modes below 120 kHz maintain nearly constant frequencies, with the primary mode being EPM, whose frequency is independent of density. For modes above 150 kHz, mode intensity weakens as EC power increases, while modes near 80 kHz and 120 kHz show intensity weakening with increasing EC power up to 234 kW, then strengthening again at 308 kW. A similar trend is observed for modes below 80 kHz. Deterioration of bulk plasma confinement is observed at ECH power levels of 308 kW, indicating that these EP-driven modes significantly affect the bulk plasma at high ECH power.

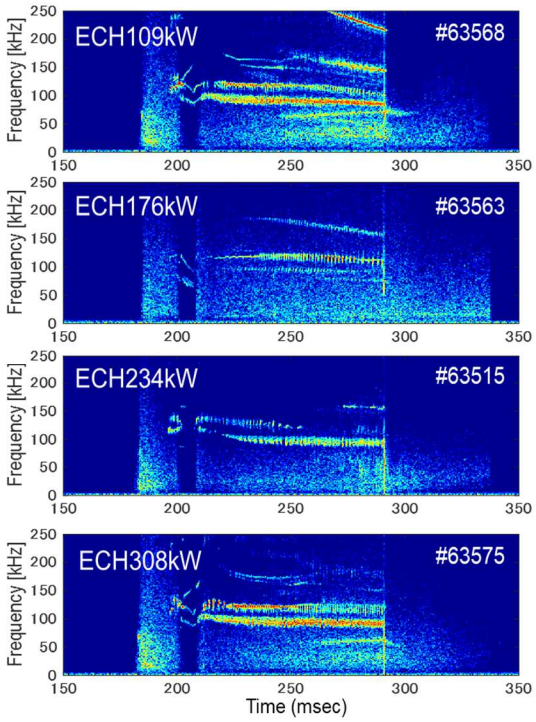

Fig. 2 Time evolution of magnetic spectrogram in medium bumpiness configuration. The EC power is scanned from 109 kW to 308 kW.

The response of EP-excited MHD instabilities to ECH varies with magnetic field configuration. Figure 3 shows the amplitude of the dominant modes observed for three types of bumpiness configurations. Mode amplitudes are evaluated from density fluctuations measured with a beam emission spectroscopy (BES) diagnostic. In the LB configuration, the mode relaxes as ECH power increases, whereas in the MB and HB configurations, the mode

behaviour is complex. In the LB configuration, all modes are mitigated with increasing EC power. In the MB configuration, on the other hand, the response of modes is contrast. The 140 kHz mode monotonically decreases in intensity with increasing ECH power, while the 80 kHz and 100 kHz modes are initially suppressed with increasing ECH power but are subsequently re-excited, indicating that an optimal ECH power exists for mode suppression. The 60 kHz mode exhibits weaker EC power dependence compared to the other modes. An experiment in the HB configuration shows a trend like that in the MB configurations: the 120kHz mode intensity monotonically decreases with ECH power, while the 60kHz, 80kHz, and 100kHz mode intensities reach their minimum at P_{EC} = 234 kW, indicating an optimum value exists for mode suppression as well as in the MB configuration. The 140 kHz mode tends to be more excited as ECH power increases.

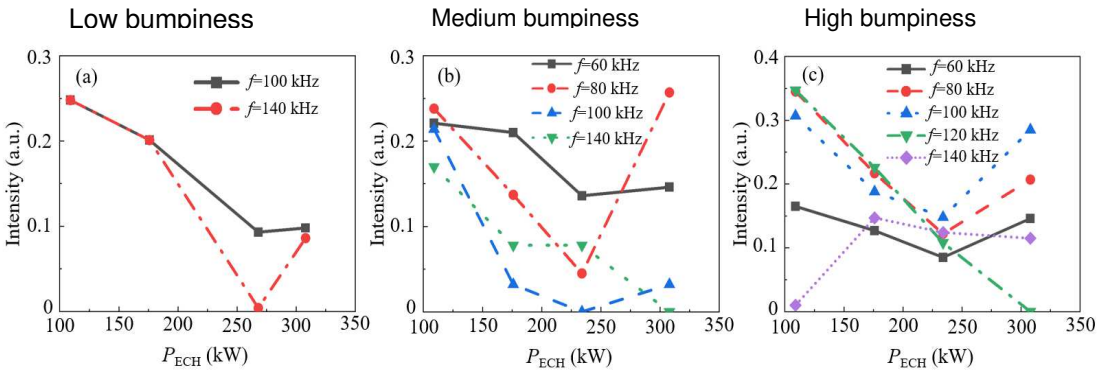

Fig. 3 Mode intensity as a function of ECH Power, at (a) low-bumpiness, (b) medium-bumpiness and (c) high-bumpiness configurations.

4. COMPARISON BETWEEN FAR3D CODE SIMULATION

Localized ECH affects mode excitation, damping, and the eigenmode itself. The stability of EP excitation modes depends not only on various damping mechanisms such as electron collision damping [41] and electron Landau damping [42], but also on continuum damping [43] via modes and continuum shifts induced by changes in pressure and plasma rotation [44][45]. Electron drag on electrons depends on T_e, altering the EP distribution gradient. AE itself is affected through coupling with acoustic waves due to changes in T_e and T_i [46]. These effects can act on the EP distribution gradient influencing mode excitation, or on the magnetic configuration affecting Alfvén continuum damping and the presence of AE in the Alfvén continuum. Non-monotonic behaviour of the EP modes may be related to the balance between excitation and damping effects induced by ECH. The ECH can change Landau damping, radiation damping, and continuum damping through the T_e change. Conversely, the change in T_e also affects the electron drag collision, which affects the slowing-down time. According to a linear theory, the increase in T_e increases the mode growth rate due to energetic ion pressure.

The FAR3d code has been applied to the Heliotron J configuration to theoretically investigate the effects of ECH, particularly identifying the MHD stability trends with respect to the EP pressure, β_f, EP slowing-down time and thermal pressure, β_{th}. Included are the effect of the plasma resistivity, the continuum, FLR and e-i Landau damping effects. The FAR3d gyro-fluid code [47][48][49][50] solves the reduced linear resistive MHD equations coupled with the EP density and parallel velocity equations [51][52][53]. The FAR3d code includes the linear wave-particle resonance to reproduce the Landau damping/growth by Landau closure relations, analysing the evolution of six field variables in a 3-D equilibria generated by the VMEC code [48]. Furthermore, the FAR3D program

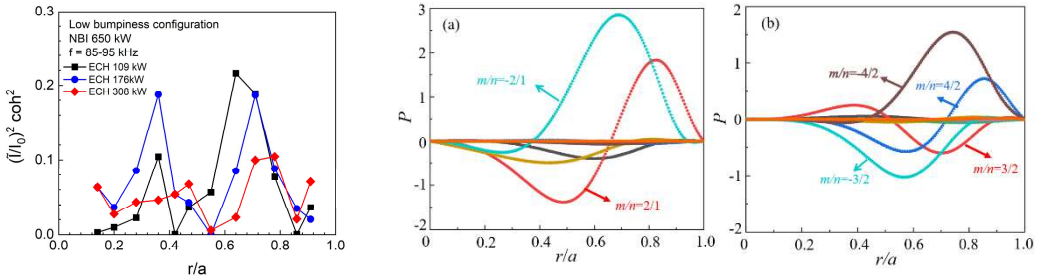

Fig. 4 Radial mode structures, (a) experimental results measured with BES at low-bumpiness configuration, and (b)n/m =1/2, 2/3 and 2/4 modes simulated by FAR3d code.

incorporates momentum equations for energetic ion density and parallel velocity, enabling the treatment of resonance effects between linear waves and ions.

Comparison of the radial mode structure has been performed. Figure 4(a) shows the radial profile of an EP-driven mode experimentally measured with the BES diagnostic in the LB configuration. The mode excited at 85–95 kHz has a mode number n/m = 1/2 according to magnetic probe measurements. When the ECH power is below 176 kW, this mode exhibits a radial structure with two peaks at r/a = 0.35 and 0.65. The linear simulations using the FAR3d code has confirmed that eigenfunctions with the same mode number exhibit similar profiles at 81 kHz, as shown in Fig. 4(b). In the n = 2 mode family, the mode with the frequency closest to the experimental value and the maximum mode intensity is found to be n/m = 2/4. This mode exhibits a double-peak structure, with the maximum amplitude distributed primarily in the central region (r/a = 0.58) and the peripheral region (r/a = 0.82). In contrast, the peak of the n/m = 2/3 mode is located mainly in the peripheral region (r/a = 0.7).

Although ECH does not directly act on EPs, it indirectly modulates the resonance conditions between EPs and modes by affecting background parameters such as T_e and particle slowing-down time, thereby influencing the driving and damping capabilities of EPs. During the heating process, the rise in T_e prolongs the EP slowing-down time, increases the EP density and EP ratio pressure, β_f, and enhances the driving force. Furthermore, the increase in plasma pressure due to heating raises the thermal particle pressure, β_{th}. By altering the MHD equilibrium, this shifts the Alfvén spectrum into the continuous spectrum decay region, reducing the overall possibility of inducing modes. Additionally, the rise in T_e decreases the plasma resistivity.

The characteristics of the mode growth rate and frequency with respect to EP pressure ratio, β_f, have been investigated. Figure 5 shows the variation in growth rate, γ for typical modes at n/m = 1/2, 2/3, and 2/4 with changes in β_f. The growth rate γ in the LB configuration for the n/m = 1/2 mode exhibits a non-monotonic trend, first decreasing and then increasing. Within the range $\beta_f \lesssim 0.6$ %, γ decreases slightly, but begins to rise sharply when βf exceeds 0.6 %. This indicates the existence of a certain drive threshold for this type of mode excitation. When the energetic particle pressure exceeds a critical value, high-intensity modes are effectively excited. For MB and HB configurations, γ gradually increases with increasing β_f. In contrast, the n/m=2/3 mode shown in Fig. 5(b) exhibits entirely different response behaviour. For LB and MB configurations, γ monotonically decreases with increasing β_f, indicating this mode is decay-dominated during the EP excitation process. Conversely, for the HB configurations, γ first increases with β_f and then shows a saturation tendency. Figure 5(c) shows the growth rate change for the n/m = 2/4 mode. For all magnetic field configurations, the growth rate of this mode increases almost linearly with increasing β_f.

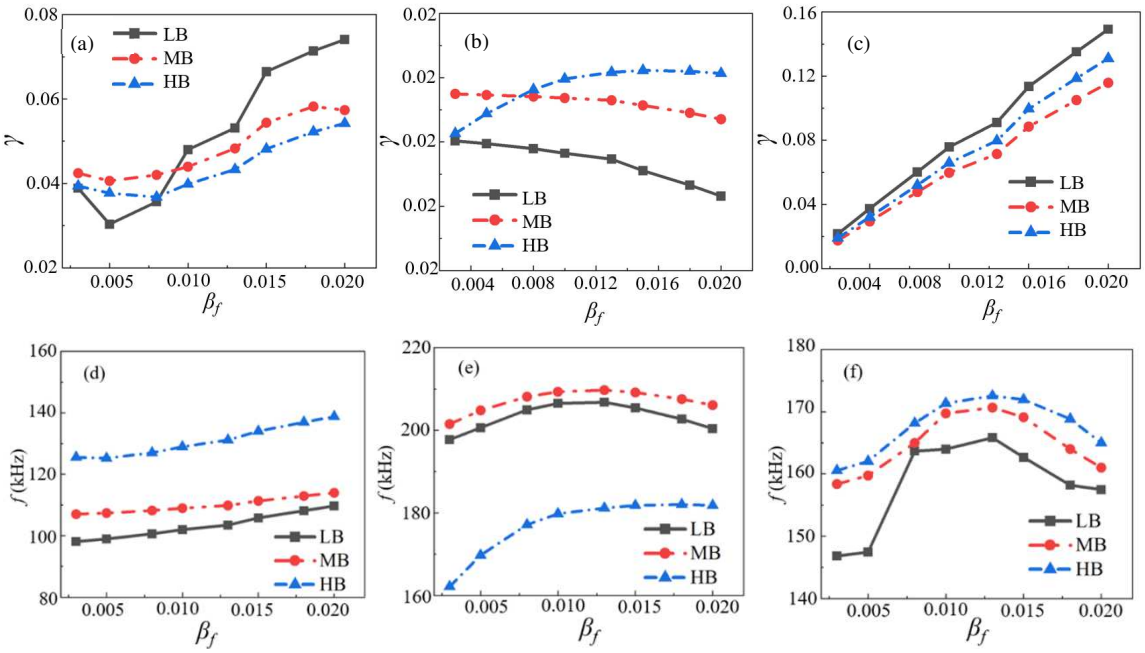

Fig. 5 Dependence of growth rate and mode frequency on energetic ion pressure in three bumpiness configurations in FAR3d code simulation, the growth rate of (a) n/m =1/2, (b) n/m =2/3, (c) n/m = 2/4, and the mode frequency of (d) n/m = 1/2, (e) n/m = 2/3, (f) n/m = 2/4.

The growth rate γ of the EP mode is determined as a function of the thermal particle beta, β_{th}. Figure 6 shows simulation results for the growth γ of each mode as a function of β_{th} for the three bumpiness configurations. This figure reveals that in LB configuration, the growth rates of the *n/m* = 1/2 and *n/m* = 2/3 modes decrease with increasing β_{th}, while the growth rate of the *n/m* = 2/4 mode remains nearly constant. In the MB configuration, the growth rate of the *n/m* = 2/3 mode remains nearly constant, while those of the *n/m* = 1/2 and *n/m* = 2/4 modes decrease with increasing β_{th}. The *n/m* = 1/2 mode is completely suppressed in the MB configuration when β_{th} exceeds a certain threshold, causing its growth rate to drop to zero. This result may explain the suppression of the *n/m* = 1/2 mode observed experimentally in MB configuration. For the HB configurations, only the *n/m* = 2/3 mode exhibits a decrease in growth rate with increasing β_{th}, while no significant change is observed in the other two modes.

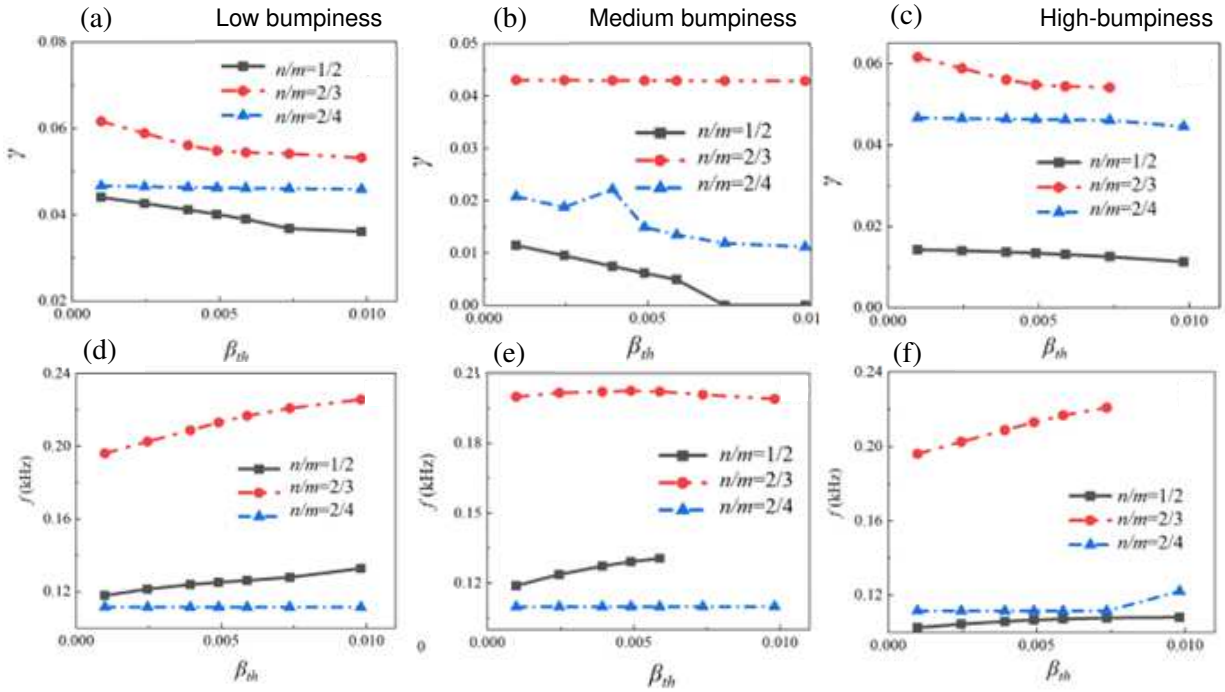

Fig. 6 Dependence of growth rate and mode frequency on thermal ion pressure in FAR3d code simulation, the growth rate in (a) low-bumpiness, (b) medium-bumpiness and (c) high-bumpiness configurations, and the mode frequency of (d) low-bumpiness, (b) medium-bumpiness and (c) high-bumpiness configurations.

The dependence of the mode growth rate and frequency on the resistivity is also studied in the FAR3d code. Figure 7 show the mode growth rate and frequency of the *n* = 1 and *n* = 2 modes as a function of Reynolds number, *S*. The dependence on the resistivity is very weak, indicating that the resistivity change due to the ECH does not affect the modes.

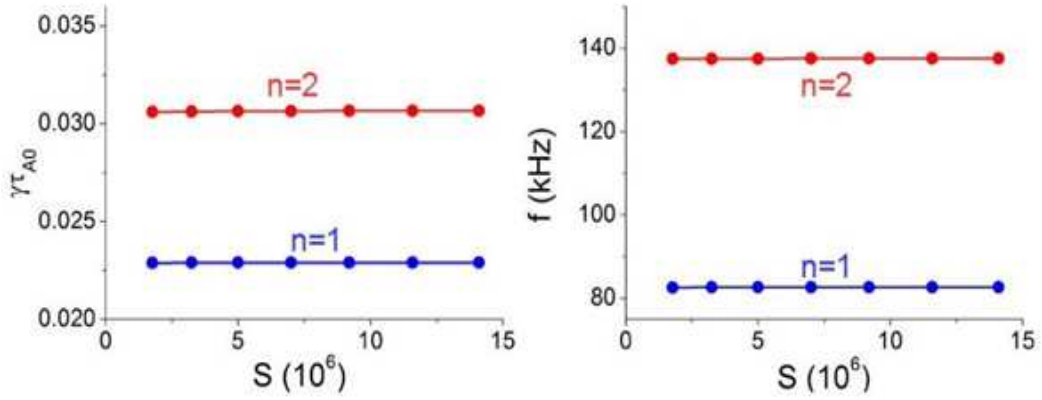

Fig. 7 Dependence of growth rate and mode frequency on resistivity in FAR3d code simulation.

Another effect influenced by changing the magnetic field configuration is the trapped electron fraction. Figure 8 shows the bumpiness dependence of the trapped electron fraction generated by ECH, calculated using a ray tracing code TRAVIS [54]. As the bumpiness increases, the trapped electron fraction increases, being approximately twice as high in the HB configuration compared to the LB configuration. This is because the magnetic field ripple structure changed, causing ECH power absorption to occur closer to the bottom of the helical ripple in the HB configuration. It is reported that collision of trapped electrons with passing electrons and ions makes the damping rate of TAE modes enhanced [41]. For typical fusion plasma condition, $v_{Te} >> v_{beam}$, electrons with $v_{\|} << v_{Te}$ can resonantly interact with EP-driven modes, and trapped electrons satisfies this condition. The damping term due to magnetic curvature drift of passing electrons can be enhanced by existence of trapped electrons. In S/H systems, the collisionless orbit transformation between the locally trapped states and locally passing states changes the collisional damping rate [55]. ECH and magnetic configuration affect the population of trapped electrons. Comparison of the mode intensity between the HB and LB configurations shows that the mode intensities in the HB configuration is lower than those in the LB configuration. This may be related to the trapped electron population, although this effect cannot simply explain the EC power dependence in all the configurations.

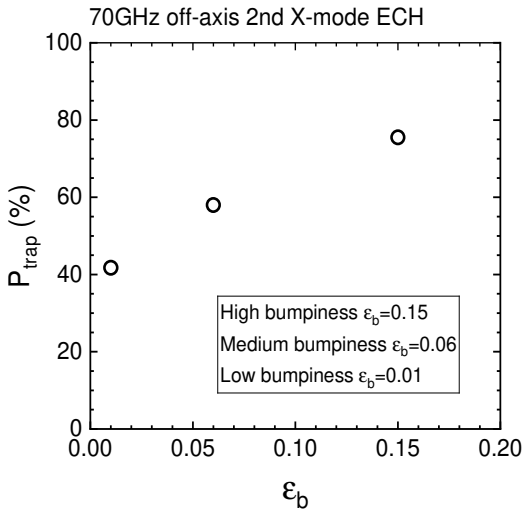

Fig. 8 Power fraction of trapped electrons in three bumpiness configuration simulated by TRAVIS code.

5. CONCLUSION

The effects of ECH and magnetic field configuration on the excitation and suppression of EP-driven MHD instabilities has been investigated in the Heliotron J device. The Heliotron J device enables to change the magnetic configuration, particularly the bumpiness (toroidal mirror ripple) components, which may provide the possibility of controlling and understanding the EP modes. We have demonstrated that mode excitation and suppression depend on the magnetic field configuration, and that the effect on ECH varies depending on the excited modes. For some specific modes, an optimal ECH output exists for mitigation, as the mode intensity decreases most significantly at a certain ECH power level. This implies that the ECH has both stabilizing and destabilizing effects. The radial distribution of the mode exhibited a multi-peak radial structure, consistent with eigenvalue calculations using the FAR3d code. Linear growth rate calculations using the FAR3d code indicate that the dependence of the growth rate of modes on EP beta depends on magnetic configuration, qualitatively explaining the experimental results. The simulation results also show that the growth rate of some modes is sensitive to changes in the thermal particle beta as well as the effect of energetic particle beta being particularly strong. Changes in resistivity do not affect the linear growth rate so much. The trapped electron fraction may have a role on the mode stability.

ACKNOWLEDGEMENTS

The authors are grateful to the Heliotron J group for their support in conducting the experiment. This work was conducted with support from the NIFS Collaborative Research Program (NFIS10KUHL030), Grant-in-Aid for Scientific Research, MEXT (Kiban (A) 22H00117), and JSPS Core-to-Core Program, A. Advanced Research Networks, PLADyS, and the National Key R&D Program of China (Grant No. 2019YFE03090100).

REFERENCES

[1] Heidbrink W. 2008 Phys. Plasmas 15 055501
[2] Breizman B.N. and Sharapov S.E., 2011 Plasma Phys. Control. Fusion 53 054001
[3] Toi K. et al 2011 Plasma Phys. Control Fusion 53 024008
[4] Salewski M. et al 2025 Nucl. Fusion 65 043002
[5] Fasoli, A. et al 2002 Plasma Phys. Control. Fusion 44 B159–B172

[6] Sharapov S.E. et al. 2018 Nucl. Fusion 58 082008
[7] Herrmann M.C. and Fisch N.J., 1997 Phys. Rev. Lett. 79 1495
[8] Fisch N.J. 2015 AIP Conf. Proc. 1689 020001
[9] Garcia-Munoz M. et al 2019 Plasma Phys. Control. Fusion 61 054007
[10] Pace D.C. et al 2017 Nucl. Fusion 57 014001
[11] Podesta M. et al 2010 Phys. Plasmas 17 122501
[12] Fredrickson E.D. et al 2015 Nucl. Fusion 55 013012
[13] Fredrickson E.D. et al 2017 Phys. Rev. Lett. 118 265001
[14] Heidbrink W.W. et al 2013 Nucl. Fusion 53 093006
[15] Turnyanskiy M. et al 2013 Nucl. Fusion 53 053016
[16] Van Zeeland M.A. et al 2008 Plasma Phys. Control. Fusion 50 035009
[17] Van Zeeland M.A. et al 2016 Nucl. Fusion 56 112007
[18] Garcia-Munoz M. et al 2015 Impact of localized ECRH on NBI and ICRH driven Alfvén eigenmodes in the ASDEX Upgrade tokamak 14th IAEA Technical Meeting on Energetic Particles (Vienna, Austria, 3 September 2015)
[19] Sharapov S.E. et al 2018 Plasma Phys. Control. Fusion 60 014026
[20] Lazaros A. et al 2002 Phys. Plasmas 9 3007
[21] Nagaoka K. et al 2013 Nucl. Fusion 53 072004
[22] Melnikov A.V. et al 2016 Nucl. Fusion 56 112019
[23] Melnikov A. et al 2018 Plasma Phys. Control. Fusion 60 084008
[24] Nagasaki K. et al 2013 Nucl. Fusion 53 113041
[25] Yamamoto S. et al 2017 Nucl. Fusion 57 126065
[26] Bortolon A. 2013 Phys. Rev. Lett. 110 265008
[27] Kramer G.J. et al 2016 Plasma Phys. Control. Fusion
[28] Prater R 2004 Physics of Plasmas 11 2349
[29] Cappa A. et al 2021 Nucl. Fusion 61 066019
[30] Varela J. et al 2020 Nucl. Fusion 60 046013
[31] Yamamoto S. et al 2020 Nucl. Fusion 60 066018
[32] Van Zeeland M.A. et al 2008 Plasma Phys. Control. Fusion 50 035009
[33] Sharapov S.E. et al 2018 Plasma Phys. Control. Fusion 60 14026
[34] Garcia-Munoz M. et al 2015 IAEA TM Energetic Particles in Magnetic Confinement Systems (IAEA HQ, Vienna, 4–7 September 2015)
[35] Varela J et al 2023 Nucl. Fusion 63 026009
[36] Zhong Y. et al. 2024 Plasma Fus. Res. 19 1202008
[37] Obiki T et al 2001 Nuclear Fusion 41 833
[38] Wakatani M. et al 2000 Nucl. Fusion 40 569
[39] Mizuuchi T. et al 2006 Fus. Sci. Tech. 50 352
[40] Spong D A, et al 2003 Physics of Plasmas 10 3217
[41] Gorelenkov N.N. and Sharapov S.E. 1992 Phys. Scr. 45 163
[42] Chen L. and Zonca F. 2017 Phys. Plasmas 24 072511
[43] Berk H.L., Van Dam J.W., Guo Z. and Lindberg D.M. 1992 Phys. Fluids B 4 1806–35
[44] Podestà M. et al 2010 Phys. Plasmas 17 122501
[45] Saigusa M. et al 1997 Nucl. Fusion 37 1559
[46] Chu M.S. et al 1992 Phys. Fluids B 4 3713–21
[47] Garcia L. 1998 June 29 - July 3 Proc. 25th EPS Int. Conf. (Prague) vol 22A p 1757 http://ocs.ciemat.es/EPS1998/start.htm
[48] Charlton L.A., Holmes J.A., Hicks H.R., Lynch V.E. and Carreras B.A. 1986 J. Comput. Phys. 63 107
[49] Charlton L.A., et al 1990 J. Comput. Phys. 86 270
[50] Varela J., Spong D.A. and Garcia L. 2017 Nucl. Fusion 57 126019
[51] Spong D.A., Carreras B.A. and Hedrick C.L. 1994 Phys. Plasmas 1 1503
[52] Spong D.A. et al 2014 Plasma Fusion Res. 9 3403077
[53] Hedrick C.L., Leboeuf J.-N. and Spong D.A. 1992 Phys. Fluids B 4 3869
[54] Nagasaki K. et al 2011Nucl. Fusion 51 103035
[55] Kolesnichenko Ya. I. 2004 Phys. Plasmas 11 4616